

Trajectory-Diversity-Driven Robust Vision-and-Language Navigation

Jiangyang Li¹ Cong Wan¹ Songlin Dong^{1,2*} Chenhao Ding¹ Qiang Wang¹
Zhiheng Ma² Yihong Gong^{1,2}

¹Xi'an Jiaotong University

²Faculty of Computility Microelectronics, Shenzhen University of Advanced Technology

Abstract

Vision-and-Language Navigation (VLN) requires agents to navigate photo-realistic environments following natural language instructions. Current methods predominantly rely on imitation learning, which suffers from limited generalization and poor robustness to execution perturbations. We present NavGRPO, a reinforcement learning framework that learns goal-directed navigation policies through Group Relative Policy Optimization. By exploring diverse trajectories and optimizing via within-group performance comparisons, our method enables agents to distinguish effective strategies beyond expert paths without requiring additional value networks. Built on ScaleVLN, NavGRPO achieves superior robustness on R2R and REVERIE benchmarks with +3.0% and +1.71% SPL improvements in unseen environments. Under extreme early-stage perturbations, we demonstrate +14.89% SPL gain over the baseline, confirming that goal-directed RL training builds substantially more robust navigation policies. Code and models will be released.

1. Introduction

Vision-and-Language Navigation (VLN) [5] is a core task in Embodied AI, requiring agents to autonomously navigate to target locations based on natural language instructions. This task is highly challenging as agents must ground abstract linguistic concepts to visual observations and perform multi-step reasoning to achieve navigation goals. Additionally, VLN tasks typically require agents to execute instructions in unseen environments, posing stringent tests on the model’s generalization capability.

Currently, the mainstream paradigm for solving VLN tasks is imitation learning (IL), which employs DAgger-based [13] techniques to train agents to mimic expert demonstrations through supervised learning. Although these methods have achieved significant results in seen en-

vironments, their optimization objective is to imitate expert behavior rather than learn goal-directed reasoning. Therefore, two fundamental limitations exist: (i) Limited generalization capability: IL agents rely on expert trajectories in training data, leading to overfitting and difficulty generalizing to unseen environments. (ii) Poor robustness to perturbations: IL methods suffer from the inherent distribution shift problem. When agents deviate from expert paths due to perturbations, they enter unseen state distributions. Without effective recovery policies, such deviations often prevent task completion.

Figure 1 intuitively shows that in unseen environments, when IL agents are perturbed and deviate from expert paths, they often have to take significant detours due to a lack of effective recovery strategies. This raises the core question of this paper: *Can we train a VLN agent that not only overcomes the limited generalization capability of IL, but also possesses effective recovery and replanning capabilities when perturbed and deviating from expert paths?*

We hypothesize that robust learning requires exposing agents to **diverse navigation trajectories**, including both successes and failures. By learning relative distinctions across all outcomes, rather than relying solely on the absolute correctness of expert demonstrations, an agent can extract a richer learning signal that generalizes beyond simple expert replication.

To realize this hypothesis, we propose NavGRPO, a reinforcement learning framework designed for robust generalization built on three key design choices. (1) Group Relative Policy Optimization [22]. GRPO samples multiple trajectories per instruction and optimizes policies through within-group performance comparisons. Unlike value-based RL methods [12] that require auxiliary critic networks, GRPO directly learns from trajectory-level rewards by ranking outcomes within each group. This design naturally encourages exploration of diverse navigation strategies while avoiding the instability of value network training, enabling agents to discover effective recovery behaviors beyond expert demonstrations. (2) Goal-oriented trajectory reward. Unlike prior RL methods using step-wise rewards [90],

*Corresponding author.

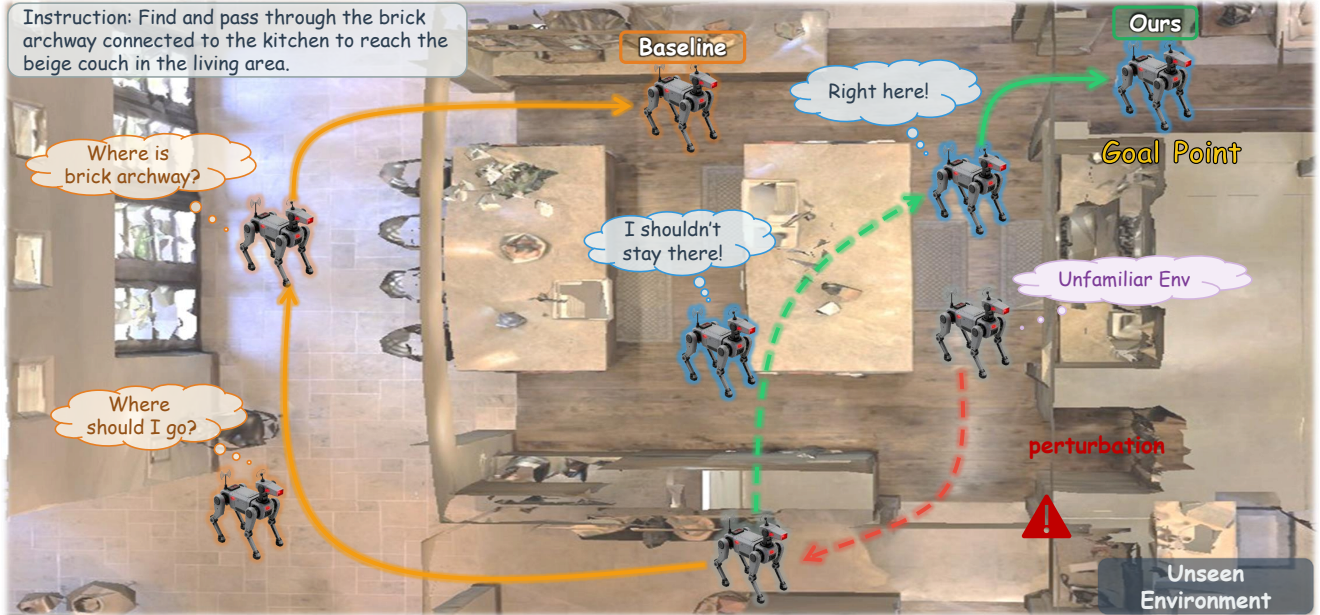


Figure 1. Navigation behavior under early-stage perturbations in unfamiliar environments. The baseline IL agent struggles to recover from errors due to limited exposure to failed trajectories, often detouring or failing to reach the goal. Our NavGRPO agent learns from diverse rollouts, enabling robust error correction and successful navigation despite perturbations.

our reward directly evaluates complete trajectories based on goal achievement and path efficiency, providing clearer learning signals. (3) Adaptive training strategy. We incorporate targeted supervised fine-tuning on challenging instructions to prevent catastrophic forgetting and complement reinforcement learning with behavioral guidance.

On R2R [5] and REVERIE [71] validation unseen splits, we achieve +3% and +1.71% SPL improvements over the ScaleVLN baseline. More importantly, under extreme perturbations where agents are forced off-path in early steps, we demonstrate superior robustness with +14.89% SPL improvement compared to ScaleVLN, showing effective robustness. Our contributions are: (1) We establish an effective framework for VLN that integrates GRPO with a multi-level reward function and adaptive training strategy, applicable to multiple baseline models. (2) Perturbation experiments show that agents trained with GRPO exhibit stronger robustness to perturbations present in navigation. (3) On standard R2R and REVERIE unseen benchmarks, we provide empirical evidence that goal-directed RL fine-tuning improves generalization to unseen environments.

2. Related Work

Vision-and-Language Navigation (VLN). VLN requires embodied agents to follow natural language instructions to reach target locations in photo-realistic environments. The task was formalized with the Matterport3D simulator [7], and various datasets have since been introduced to address

different aspects of embodied navigation [5, 36, 42, 43, 71, 108], covering diverse scenarios from fine-grained object interaction to long-horizon instruction following across indoor and outdoor scenes. Early approaches employed sequence-to-sequence architectures with imitation learning [5, 18, 49], which were later complemented by diverse training strategies including reinforcement learning [82, 89, 90], adversarial training [19, 53, 99], generative modeling [44], curriculum learning [97], and cycle-consistent learning [84]. The integration of vision-language pre-training brought substantial improvements through large-scale offline pre-training [16, 21, 23, 24, 30, 33, 59, 66, 73], auxiliary task design [48, 52, 65, 91, 107], and regularization techniques [69, 86, 92] for more stable and less biased training. Architectural innovations evolved from recurrent encoders to sophisticated representations, including attention-based mechanisms [12, 28], graph-based topological reasoning [10, 13, 17, 83], and scene representations [3, 6, 8, 57, 61, 62, 85, 94], with recent works designing flexible action spaces for efficient exploration and backtracking [13, 20, 35, 38, 81]. To enhance cross-modal understanding, researchers have pursued finer-grained visual feature extraction [31, 34, 55, 67, 72, 101] and textual decomposition [1, 15, 26, 27, 46, 54, 70, 100, 109], while incorporating external knowledge from large language models [9, 56, 64, 68, 75, 76, 104–106], vision-language models [48], and structured knowledge bases [50]. Parallel efforts in data augmentation have explored observation per-

turbation [25, 39, 47], automatic trajectory annotation via speaker-follower frameworks [18, 32, 40, 51, 80, 88, 95], and large-scale scene generation [14, 37, 45, 58, 60, 93]. Despite these advances, existing methods predominantly rely on imitation learning from expert demonstrations, limiting exposure to diverse navigation scenarios. This results in poor generalization to novel configurations and fragility under execution deviations. We address these limitations with NavGRPO, a trajectory-level reinforcement learning approach that learns from diverse navigation experiences to develop robust policies.

Reinforcement Learning for VLN. While imitation learning dominates VLN research, several efforts have explored reinforcement learning to address generalization challenges. Early work by Wang et al. [90] introduced Reinforced Cross-Modal Matching (RCM), which employs a matching critic to provide intrinsic rewards for vision-language alignment, combined with sparse task rewards through policy gradient optimization. Their method further incorporated Self-Imitation Learning (SIL) to exploit successful trajectories in unseen environments, demonstrating improved generalization on R2R. Subsequent approaches focused on reward engineering: SERL [82] proposed soft expert reward learning to distill expert demonstrations into dense reward signals, avoiding manual reward shaping while maintaining strong supervision from human annotations. More recent methods have integrated RL into their training pipelines, with HAMT [12] applying policy gradient fine-tuning after pretraining, and SEvol [8] using RL to refine graph-based scene representations. However, these methods face critical limitations: step-level sparse rewards lead to severe credit assignment issues in long-horizon navigation, while learned value networks struggle in VLN’s high-dimensional action space. We adopt Group Relative Policy Optimization (GRPO) [22], which eliminates both issues through trajectory-level geometric rewards and advantage estimation via relative ranking, enabling robust learning from diverse trajectories including both successful and failed attempts.

3. Method

Problem Definition. In the standard VLN setup, the environment is represented as an undirected navigation graph $\mathcal{G} = \{\mathcal{V}, \mathcal{E}\}$, where $\mathcal{V} = \{V_i\}_{i=1}^K$ denotes a set of K navigable locations and \mathcal{E} represents the connectivity edges between locations. Each location in the graph corresponds to a specific viewpoint in the physical environment, and the agent can only traverse along the edges defined by the graph structure. Given a natural language instruction $\mathcal{W} = \{w_1, w_2, \dots, w_L\}$ composed of L words, at each navigation timestep t , the agent is situated at location $V_t \in \mathcal{V}$ and perceives the surrounding environment through panoramic visual observations $\mathcal{O}_t = \{o_i\}_{i=1}^n$ captured at the current

location, consisting of n view images. The agent also observes a set of reachable neighboring nodes $\mathcal{N}(V_t)$. Based on the instruction and current observations, the agent must select an action a_t from the available action space \mathcal{A}_t . The action space includes navigating to a neighboring location $V_{t+1} \in \mathcal{N}(V_t)$ connected to the current position, or issuing a stop signal to terminate the navigation episode.

Overview. NavGRPO trains navigation policies through Group Relative Policy Optimization, which learns from diverse trajectories sampled during training. We describe the GRPO framework in Sec. 3.1, our geometric reward design in Sec. 3.2, and the training pipeline in Sec. 3.3.

3.1. NavGRPO for VLN

We adopt GRPO [22], which estimates advantages through group-based reward comparison without requiring a separate value network.

Policy Architecture. The proposed navigation policy π_θ is parameterized by the vision-language transformer network. At each timestep t , given the instruction \mathcal{W} , the current panoramic observations \mathcal{O}_t , and the graph map representation \mathcal{M}_t that encodes spatial topology and historical navigation information, the policy outputs a probability distribution over the action space:

$$\pi_\theta(a_t|\mathcal{W}, \mathcal{O}_t, \mathcal{M}_t) = \text{softmax}(f_\theta(\mathcal{W}, \mathcal{O}_t, \mathcal{M}_t)) \quad (1)$$

where f_θ represents the network’s logit output for each candidate action in \mathcal{A}_t .

Group-based Trajectory Sampling. For each instruction \mathcal{W}_i sampled from the instruction set \mathcal{D}_B , which denotes a mini-batch of B instructions, we sample a group of K independent trajectories by rolling out the current policy π_θ . Each trajectory $\tau_k = (s_{k,0}, a_{k,0}, s_{k,1}, a_{k,1}, \dots, s_{k,T})$ represents a complete navigation episode, where $s_{k,t} = (V_{k,t}, \mathcal{O}_{k,t}, \mathcal{M}_{k,t})$ denotes the state at timestep t . During sampling, actions are drawn stochastically from $a_t \sim \pi_\theta(\cdot|s_{k,t})$, and we store the corresponding log probability $\log \pi_\theta(a_{k,t}|s_{k,t})$ as $p_{k,t}^{\text{old}}$ for later policy updates.

Debiased Group Relative Advantage Estimation. For each instruction \mathcal{W} in the training batch, we sample K trajectories and compute their rewards $\{r_1, r_2, \dots, r_K\}$ using the reward function detailed in Section 3.2. Following Dr.GRPO [63], we estimate advantages through group-relative comparison without variance normalization:

$$\hat{A}_k = r_k - \text{mean}(\{r_1, \dots, r_K\}) \quad (2)$$

This uses the empirical group mean as a natural baseline, eliminating the need for separate value function approximation. Removing variance normalization avoids amplifying noise in low-diversity groups, making the learning signal more robust. The trajectory-level advantage is broadcast to all timesteps during policy updates.

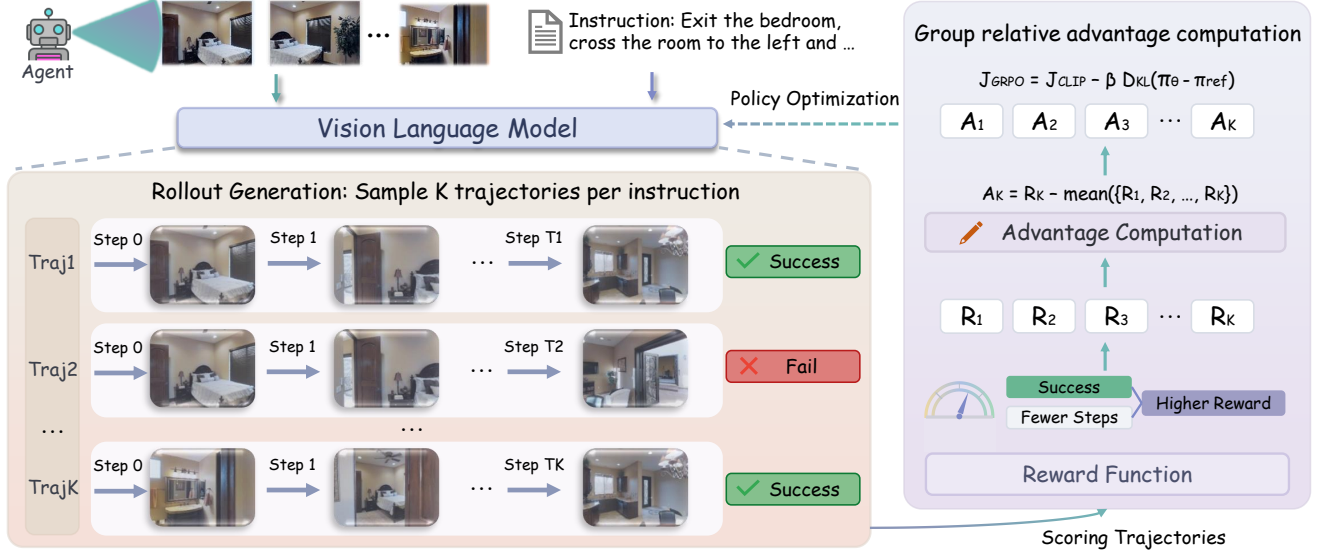


Figure 2. Overview of our NavGRPO training framework for vision-language navigation. For each instruction, we sample K diverse trajectories through policy rollout, compute rewards using trajectory-level and step-level signals, estimate group relative advantages by comparing within instruction groups, and optimize the policy through debiased advantage estimation without value networks.

Policy Optimization Objective. For each state-action transition $(s_{k,t}, a_{k,t})$ in trajectory τ_k , we compute the probability ratio:

$$\rho_{k,t} = \frac{\pi_{\theta}(a_{k,t}|s_{k,t})}{\pi_{\theta_{\text{old}}}(a_{k,t}|s_{k,t})} = \exp(\log \pi_{\theta}(a_{k,t}|s_{k,t}) - p_{k,t}^{\text{old}}) \quad (3)$$

where $\pi_{\theta_{\text{old}}}$ represents the behavior policy with frozen parameters. We incorporate the step-level progress coefficient $\gamma_{k,t}$ from Section 3.2 to modulate the advantage signal. Following PPO [79], the clipped surrogate objective becomes:

$$\mathcal{J}_{\text{clip}}(k, t) = \min\left(\gamma_{k,t} \hat{A}_k \rho_{k,t}, \gamma_{k,t} \hat{A}_k \cdot \text{clip}(\rho_{k,t}, 1-\delta, 1+\delta)\right) \quad (4)$$

The clipping mechanism constrains $\rho_{k,t}$ within $[1-\delta, 1+\delta]$ to prevent excessively large policy updates. The complete optimization objective is:

$$\mathcal{J}_{\text{GRPO}}(\theta) = \mathbb{E}_{\mathcal{W} \sim \mathcal{D}_{\mathcal{B}}, \{\tau_k\}_{k=1}^K \sim \pi_{\theta_{\text{old}}}(\cdot|\mathcal{W})} \left[\frac{1}{K} \sum_{k=1}^K \sum_{t=1}^{|\tau_k|} (\mathcal{J}_{\text{clip}}(k, t) - \beta \mathbb{D}_{\text{KL}}[\pi_{\theta} \|\pi_{\text{ref}}]) \right] \quad (5)$$

We aggregate across all timesteps without length normalization to avoid introducing bias. The KL divergence term regularizes the policy against the reference policy π_{ref} , which is the fixed policy before RL training begins, weighted by β to prevent excessive deviation.

3.2. Reward Function for NavGRPO

The reward function guides the RL training process by providing learning signals at both trajectory and step levels. We design a composite reward function with trajectory-level rewards for overall navigation quality and step-level rewards for step-wise progress.

Navigation Success Reward. Let V_T^k denote the final viewpoint of trajectory τ_k and V^* represent the target destination. The navigation error is $d_k = d_{\text{shortest}}(V_T^k, V^*)$. The success reward uses exponential decay:

$$R_{\text{nav}}(d_k) = \exp\left(-\frac{d_k^2}{2\epsilon^2}\right) \cdot \mathbb{I}(d_k < \epsilon) \quad (6)$$

Where ϵ is the success threshold. This provides smooth decay that emphasizes precise goal reaching while maintaining differentiability.

Path Efficiency Reward. To discourage inefficient behaviors such as backtracking and detours, we penalize excessive path length:

$$R_{\text{path}}(L_k, L^*) = -\max(L_k - L^*, 0)/L^* \quad (7)$$

where L_k is the actual path length and L^* is the shortest path length.

Total Reward Function. The trajectory-level reward combines navigation success and path efficiency:

$$r_k = R_{\text{nav}}(d_k) + \alpha \cdot R_{\text{path}}(L_k, L^*) \quad (8)$$

where α balances the contribution of path efficiency.

Table 1. Robustness analysis under stochastic perturbations on R2R Val Unseen. Left: Global perturbation samples from policy distribution with probability p . Right: Early perturbation selects the least probable action for the first N steps. Δ SPL shows SPL degradation from the unperturbed setting (prob=0 or Steps=0) for each method. NavGRPO demonstrates superior robustness across all perturbation levels.

Method	Global Perturbation						Early Perturbation					
	prob	OSR \uparrow	NE \downarrow	SR \uparrow	SPL \uparrow	Δ SPL	Steps	OSR \uparrow	NE \downarrow	SR \uparrow	SPL \uparrow	Δ SPL
ScaleVLN	0.0	87.48	2.34	79.40	69.97	-0.00	0	87.48	2.34	79.40	69.97	-0.00
NavGRPO	0.0	89.18	2.19	81.88	72.65	-0.00	0	89.18	2.19	81.88	72.65	-0.00
ScaleVLN	0.2	87.14	2.43	78.97	67.80	-2.17	1	83.06	2.94	74.76	59.06	-10.91
NavGRPO	0.2	88.75	2.21	81.27	72.11	-0.54	1	85.05	2.67	77.44	67.04	-5.61
ScaleVLN	0.4	87.19	2.42	78.67	65.90	-4.07	2	83.61	2.86	75.69	54.25	-15.72
NavGRPO	0.4	88.79	2.22	81.06	71.69	-0.96	2	83.85	2.70	76.50	65.10	-7.55
ScaleVLN	0.8	87.06	2.52	77.61	61.94	-8.03	3	83.52	3.04	74.16	47.77	-22.20
NavGRPO	0.8	88.49	2.27	79.95	69.98	-2.67	3	82.96	2.82	75.35	62.66	-9.99

Step-level Progress Coefficient. Navigation tasks possess well-defined spatial metrics that allow quantifying progress at each decision step. For trajectory τ_k at timestep t , we define a progress coefficient that modulates the advantage signal:

$$\gamma_{k,t} = 1 + \text{sign}(\hat{A}_k) \cdot \frac{d_{t-1} - d_t}{L^*} \quad (9)$$

where d_t is the distance to the goal at step t and L^* is the ground-truth shortest path length. This coefficient ensures that steps approaching the goal ($d_{t-1} > d_t$) yield stronger learning signals $\gamma_{k,t} \cdot \hat{A}_k$ in magnitude, while steps deviating from the goal receive attenuated signals, allowing the agent to distinguish productive actions even in failed trajectories.

3.3. Adaptive Training with Hard Case Replay

While our method enables learning from diverse trajectories, certain instructions remain persistently challenging despite extensive sampling. We address this by periodically applying supervised refinement on hard cases identified during RL training.

Hard Case Identification. For each instruction \mathcal{W}_i in the training batch, we sample K trajectories and identify it as a hard case when all sampled trajectories fail:

$$\text{Hard}(\mathcal{W}_i) = \mathbb{I} \left(\sum_{k=1}^K \mathbb{I}(d_k < \epsilon) = 0 \right) \quad (10)$$

These instructions are stored in buffer $\mathcal{B}_{\text{hard}}$.

Supervised Refinement. When $|\mathcal{B}_{\text{hard}}|$ reaches threshold M , we perform supervised updates on expert trajectories:

$$\mathcal{L}_{\text{hard}}(\theta) = -\frac{1}{|\mathcal{B}_{\text{hard}}|} \sum_{\mathcal{W}_i \in \mathcal{B}_{\text{hard}}} \sum_{t=0}^{T_i} \log \pi_{\theta}(a_t^* | s_t^*, \mathcal{W}_i) \quad (11)$$

The buffer is then cleared. This adds negligible cost since the compute saved from fewer RL rollouts more than compensates for the supervised updates on hard cases.

4. Experiment

4.1. Experimental Setup

Datasets. We evaluate on three widely-used VLN benchmarks: R2R [5] provides fine-grained step-by-step navigation instructions; REVERIE [71] presents high-level goal-oriented instructions specifying target rooms and objects; R2R-CE [42] extends R2R to continuous environments using Habitat simulator [78], where agents navigate continuously rather than between discrete viewpoints.

Evaluation Metrics. We adopt standard VLN evaluation metrics [5]. Navigation Error (NE) measures the average distance in meters between the agent’s final position and the goal location. Success Rate (SR) computes the percentage of episodes where the agent stops within 3 meters of the target. Success Rate penalized by Path Length (SPL) penalizes SR by the ratio of the shortest path length to the actual trajectory length, rewarding both accuracy and efficiency. Oracle Success Rate (OSR) measures the success rate under an ideal stop policy.

Implementation Details. We maintain the same setup as baseline methods [13, 93]. All models are trained for 200k steps with learning rate 1×10^{-5} . After supervised warm-up (30k steps), we transition to GRPO with batch size $B = 8$ and $K = 8$ trajectories per instruction. Following standard PPO settings [79], we set clipping threshold $\delta = 0.2$ and KL penalty $\beta = 0.01$. For reward function, we use $\alpha = 0.25$. For hard case replay, we set buffer size $M = 200$. As training progresses and the policy improves, the frequency of hard case updates naturally decreases. All results are averaged over three random seeds.

4.2. Robustness to Action Noise

Motivation. Real-world deployment faces execution noise from sensor errors and actuation imprecision. While imitation learning optimizes for near-optimal trajectories, it provides limited exposure to noisy action sequences during

Table 2. Comparison with SoTA methods on R2R and REVERIE datasets. †: Methods using reinforcement learning for policy optimization.

Methods	R2R Val Unseen			R2R Test Unseen			REVERIE Val Unseen			REVERIE Test Unseen		
	NE↓	SR↑	SPL↑	NE↓	SR↑	SPL↑	OSR↑	SR↑	SPL↑	OSR↑	SR↑	SPL↑
RCM† [90]	5.88	43	-	6.12	43	38	14.23	9.29	6.97	11.68	7.84	6.67
SERL† [82]	4.74	56	48	5.63	53	49	-	-	-	-	-	-
VLN○BERT [28]	3.93	63	57	4.09	63	57	35.02	30.67	24.90	32.91	29.61	23.99
HAMT† [12]	3.65	66	61	3.93	65	60	36.84	32.95	30.20	33.41	30.40	26.67
SEvol† [8]	3.99	62	57	4.13	62	57	-	-	-	-	-	-
HOP+ [74]	3.49	67	61	3.71	66	60	40.04	36.07	31.13	35.81	33.82	28.24
BEVBert [3]	2.81	75	64	3.13	73	62	56.40	51.78	36.37	57.26	52.81	36.41
LANA [91]	-	68	62	-	65	60	38.54	34.00	29.26	36.41	33.50	26.89
KERM [50]	3.22	72	61	3.61	70	59	55.21	50.44	35.38	57.58	52.43	39.21
GridMM [94]	2.83	75	64	3.35	73	62	57.48	51.37	36.47	59.55	53.13	36.60
NavILLM [104]	3.51	67	59	3.71	68	60	52.27	42.15	35.68	51.75	39.80	32.33
NavGPT-2 [106]	2.84	74	61	3.33	72	60	-	-	-	-	-	-
VER [62]	2.80	76	65	2.74	76	66	61.09	55.98	39.66	62.22	56.82	38.76
MAGIC-L [87]	2.22	79	70	2.75	77	69	-	-	-	-	-	-
GOAT [86]	2.40	78	68	3.04	75	65	-	53.37	36.70	-	57.72	40.53
NavQ [96]	3.06	73	63	3.30	72	63	60.47	53.22	38.89	60.39	53.29	39.50
COSMO [98]	3.15	73	61	3.43	71	58	56.09	50.81	35.93	59.33	52.53	36.12
DUET [13]	3.31	72	60	3.65	69	59	51.07	46.98	33.73	56.91	52.51	36.06
DUET-NavGRPO	3.18	74	63	3.39	71	62	53.17	49.47	35.32	58.32	54.49	38.16
ScaleVLN [93]	2.34	79	70	2.73	77	68	63.85	56.97	41.84	62.65	56.13	39.52
ScaleVLN-NavGRPO	2.19	82	73	2.52	79	70	65.19	58.91	43.55	64.21	58.25	41.34

Table 3. Navigation performance on the R2R-CE dataset. †: Methods that apply candidate waypoint predictor to support high-level action space.

Methods	Val Unseen			Test Unseen		
	NE↓	SR↑	SPL↑	NE↓	SR↑	SPL↑
LAW [77]	6.83	35	31	-	-	-
Sim2Sim [41]	6.07	43	36	6.17	44	37
MGMap [11]	6.28	39	34	7.11	35	28
CMA† [29]	6.20	41	36	6.30	38	33
VLN○BERT† [29]	5.74	44	39	5.89	42	36
GridMM† [94]	5.11	49	41	5.64	46	39
Ego ² -Map†	4.94	52	46	5.54	47	41
Reborn [2]	5.40	50	46	5.55	49	45
ETPNAV [4]	4.71	57	49	5.12	55	48
COSMO† [98]	-	47	40	-	47	40
DUET† [13]	5.26	47	39	5.82	42	36
DUET-NavGRPO†	5.02	50	42	5.64	44	38
ScaleVLN†	4.80	55	51	5.11	55	50
ScaleVLN-NavGRPO†	4.69	57	53	5.01	57	52

training. We evaluate whether RL exploration, by experiencing diverse state-action distributions, enables the agent to better handle stochastic perturbations at inference time.

Experimental Setup. We design two perturbation strategies to evaluate robustness: (1) *Global perturbation* mimics real-world random noise—at each step with probability $p \in \{0.0, 0.2, 0.4, 0.8\}$, the agent samples an action from its policy distribution $\pi(\cdot|s)$; otherwise it takes the argmax ac-

tion. (2) *Early perturbation* tests recovery from initial mistakes—the first $N \in \{1, 2, 3\}$ steps select the *least probable* action from the policy distribution, while remaining steps use argmax actions. This simulates scenarios where agents start from poor decisions due to uncertain states, such as imprecise localization, but must recover to reach the goal.

Results and Analysis. Table 1 demonstrates superior robustness of our method across both perturbation scenarios. Under global perturbation at $p = 0.4$, our method degrades by only 0.96 SPL compared to the baseline’s 4.07 degradation, representing $4.2\times$ better robustness. At $p = 0.8$, this advantage amplifies to $3.0\times$ with degradations of 2.67 versus 8.03 SPL. Notably, our method maintains 69.98 SPL at $p = 0.8$, exceeding the baseline’s unperturbed performance of 69.97. For early perturbation, perturbing the first three steps causes our method to degrade by 9.99 SPL while the baseline degrades by 22.20 SPL, yielding a $2.2\times$ robustness advantage. These results indicate that GRPO training enables effective recovery from execution perturbations through exposure to diverse trajectories.

4.3. Main Results

R2R. Table 2 shows results on the R2R dataset. Our method consistently outperforms DUET, achieving 2% higher SR and 3% higher SPL on both val unseen and test unseen splits. When applied to ScaleVLN, our approach achieves 3% SPL improvement over the baseline and outperforms GOAT by 5% on val unseen.

Table 4. Ablation study on reward function design. Experiments are conducted on R2R val unseen split.

Method #	Reward Components			R2R Val Unseen		
	R _{nav}	R _{path}	R _{step}	NE↓	SR↑	SPL↑
1	✓			2.31	80.14	71.07
2	✓	✓		2.26	81.02	71.88
3	✓		✓	2.25	81.29	71.93
4	✓	✓	✓	2.19	81.88	72.65

Table 5. Comparison of group-based policy optimization variants on R2R Val Unseen split. All methods use the same reward function and sampling strategy.

Method	OSR↑	NE↓	SR↑	SPL↑
w/o Group	87.48	2.34	79.40	69.97
GRPO [22]	88.15	2.26	80.15	71.23
GSPO [103]	88.62	2.23	80.52	71.68
GMPO [102]	88.56	2.24	80.47	71.62
Dr.GRPO [63]	89.02	2.19	81.88	72.65

REVERIE. On the REVERIE dataset, which features high-level goal-oriented instructions requiring longer-horizon planning, our approach outperforms DUET by 2.49% in SR and 1.59% in SPL on val unseen. When built upon ScaleVLN, our method further improves SR by 1.94% and SPL by 1.71%, surpassing GOAT by 6.48% in SPL. The gains are validated on test unseen, where we achieve 1.98% higher SR and 2.10% higher SPL compared to DUET. Notably, our approach substantially outperforms traditional RL-based methods such as RCM and HAMT, which face challenges from step-level sparse rewards and credit assignment in long-horizon navigation. The consistent improvements across both datasets demonstrate generalization to diverse navigation scenarios, from fine-grained step-by-step instructions to high-level goal-oriented tasks.

R2R-CE. Table 3 presents results on the continuous R2R-CE benchmark. Despite training in discrete environments, both DUET-GRPO and ScaleVLN-GRPO show consistent improvements over their respective baselines, demonstrating effective transfer to continuous navigation scenarios.

4.4. Ablation Studies and Analysis

Impact of Reward Function Design. To understand the contribution of different reward components, we conduct ablation studies on the R2R val unseen split, as shown in Table 4. Using only the navigation success reward provides a basic foundation with 71.07% SPL, demonstrating that sparse trajectory-level signals alone can guide policy learning. Incorporating the path efficiency reward improves SPL to 71.88%, indicating that penalizing unnecessarily long trajectories encourages more compact navigation behaviors. Alternatively, adding the step-level progress reward achieves 71.93% SPL, showing that fine-grained in-

Table 6. Analysis of sampling trajectory number on R2R Val Unseen split.

Trajectories	OSR↑	NE↓	SR↑	SPL↑
$K = 2$	88.28	2.31	79.98	71.02
$K = 4$	88.62	2.28	80.37	71.98
$K = 8$	89.02	2.19	81.88	72.65
$K = 16$	89.12	2.15	81.96	72.87

termediate guidance helps the agent make better local decisions. Combining all three components yields the best performance at 72.65% SPL and 81.88% SR, demonstrating that trajectory-level and step-level rewards provide complementary supervision—the former guides overall navigation quality while the latter refines individual action selections.

Impact of Group-Based Policy Optimization. We compare different variants of group-based policy optimization to validate our design choices, as shown in Table 5. Without grouping, the agent achieves 69.97% SPL on val unseen, establishing a baseline for individual trajectory optimization. Standard GRPO [22] introduces group-wise advantage normalization, improving performance to 71.23% SPL through better calibrated gradients. We evaluate three advanced variants adapted from recent LLM alignment literature: GSPO [103] shifts importance sampling and clipping to the sequence level, GMPO [102] adopts geometric mean for step-level reward aggregation, and Dr.GRPO [63] removes length and variance normalization to mitigate length bias. Dr.GRPO achieves the strongest performance with 72.65% SPL on val unseen. We adopt Dr.GRPO’s debiased advantage estimation in our framework, which removes normalization constraints and reduces hyperparameter sensitivity. This design choice reduces hyperparameter sensitivity and proves effective for generalizing across different VLN benchmarks and base models. The consistent gains across different optimization variants confirm the robustness of this approach.

Analysis of Sampling Trajectory Number. We investigate the impact of sampling trajectory number K during training, where K trajectories are sampled for each instruction to form a group for relative advantage computation. Table 6 shows the results on R2R val unseen split with different values of K . Using fewer trajectories provides limited diversity for relative comparison, resulting in suboptimal performance. Increasing K to 8 substantially improves both SR and SPL by 1.51% and 1.63% respectively compared to $K = 4$, as the agent benefits from richer comparative signals within each group. Further increasing K to 16 yields only marginal gains of 0.08% in SR and 0.22% in SPL while doubling the training time and memory cost. Therefore, we adopt $K = 8$ as our default setting to balance performance and computational efficiency.

Comparison with Alternative RL Methods. We apply

Table 7. Comparison with alternative RL methods on R2R Val Unseen split.

Method	OSR \uparrow	NE \downarrow	SR \uparrow	SPL \uparrow
SFT only	87.48	2.34	79.40	69.97
SFT+REINFORCE	87.35	2.36	79.28	69.85
SFT+A2C	87.72	2.32	79.65	70.25
SFT+PPO	88.15	2.29	79.95	70.68
SFT+GRPO	89.02	2.19	81.88	72.65

Table 8. Analysis of different training strategies on R2R Val Unseen split.

Training Strategy	OSR \uparrow	NE \downarrow	SR \uparrow	SPL \uparrow
SFT only	87.48	2.34	79.40	69.97
RL only	74.52	4.30	64.30	59.82
Sequential SFT-RL	88.95	2.22	81.25	72.08
Ours	89.02	2.19	81.88	72.65

different RL algorithms to further optimize the IL-finetuned model in Table 7 under a unified training framework. Our GRPO uses trajectory-level rewards measuring navigation success and path efficiency, which cannot be decomposed into step-level signals required for A2C and PPO’s value bootstrapping. REINFORCE, though compatible with both reward types, still fails to improve performance due to its inherently high gradient variance. Therefore, following established practices [12], we provide classical methods with step-level rewards including distance progress and orientation alignment. REINFORCE degrades performance slightly, while A2C achieves modest gains of 0.28% SPL, and PPO improves the SPL metric to 70.68%. In contrast, our GRPO achieves 72.65% SPL, outperforming PPO by a margin of 1.97%. This result demonstrates that comparing trajectories within instruction groups yields substantially more informative learning signals than optimizing trajectories independently.

Analysis of Training Strategy. Table 8 compares different training strategies to understand the contribution of each component. All methods start from the same pretrained vision-language model. Training with RL alone performs poorly without navigation-specific initialization. SFT-only training establishes a solid baseline by learning from expert demonstrations. Sequential SFT-RL improves performance to 81.25% SR and 72.08% SPL, demonstrating that RL optimization can surpass IL-finetuned models. Our approach with hard case replay further enhances results to 81.88% SR and 72.65% SPL, providing modest but consistent gains. Importantly, hard case replay is triggered only when the entire sampled group fails, thereby avoiding redundant RL exploration on persistently challenging instructions. This adaptive strategy stabilizes training and prevents catastrophic forgetting, balancing broad policy exploration with targeted supervision.

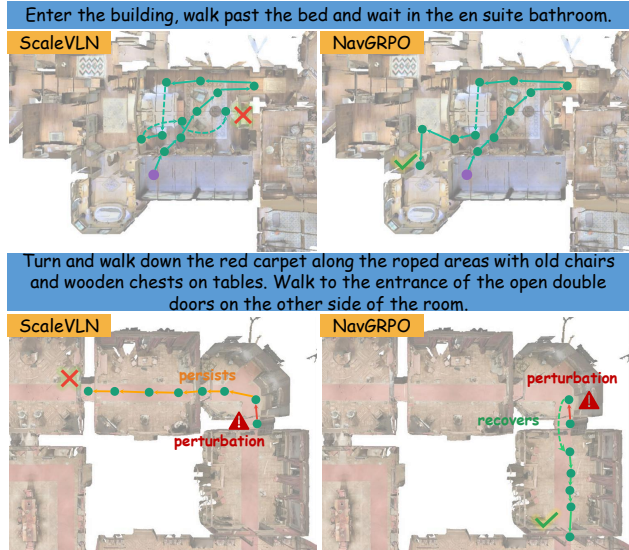


Figure 3. Qualitative comparison on challenging instructions under normal conditions (top) and initial perturbations (bottom). ScaleVLN fails to recover from errors in both scenarios. Our GRPO-trained agent successfully completes tasks and demonstrates robust error correction under perturbations.

4.5. Qualitative Analysis

Figure 3 presents qualitative comparisons on spatially ambiguous instructions. Under standard conditions, ScaleVLN commits navigation errors from which it cannot recover, while our GRPO-trained agent makes correct decisions at critical waypoints to reach target locations. Under adversarial perturbations, ScaleVLN persists along erroneous trajectories initiated by the perturbation. In contrast, our method demonstrates error-correction capabilities: in the first case, it recognizes spatial deviation and backtracks to the correct path; in the second case, it adjusts mid-trajectory despite initial disruption. This demonstrates that group-based trajectory optimization enables both improved spatial reasoning and robust recovery from navigational errors.

Additional analysis, including more RL comparisons, hyperparameter sensitivity, computational cost, visualizations, and limitations, is provided in the Appendix.

5. Conclusion

We present NavGRPO, a reinforcement learning framework for VLN that learns from diverse trajectories through Group Relative Policy Optimization. By comparing complete navigation rollouts, our method achieves stable policy updates without additional value networks. Experiments on several benchmarks show consistent improvements over imitation learning baselines, with substantial gains under perturbations, demonstrating that goal-directed RL training builds more robust navigation policies.

References

- [1] Dong An, Yuankai Qi, Yan Huang, Qi Wu, Liang Wang, and Tieniu Tan. Neighbor-view enhanced model for vision and language navigation. In *Proceedings of the 29th ACM International Conference on Multimedia*, pages 5101–5109, 2021. [2](#)
- [2] Dong An, Zun Wang, Yangguang Li, Yi Wang, Yicong Hong, Yan Huang, Liang Wang, and Jing Shao. 1st place solutions for rxr-habitat vision-and-language navigation competition (cvpr 2022). *arXiv preprint arXiv:2206.11610*, 2022. [6](#)
- [3] Dong An, Yuankai Qi, Yangguang Li, Yan Huang, Liang Wang, Tieniu Tan, and Jing Shao. Bevbert: Multimodal map pre-training for language-guided navigation. In *Proceedings of the IEEE/CVF International Conference on Computer Vision*, pages 2737–2748, 2023. [2](#), [6](#)
- [4] Dong An, Hanqing Wang, Wenguan Wang, Zun Wang, Yan Huang, Keji He, and Liang Wang. Etpnav: Evolving topological planning for vision-language navigation in continuous environments. *IEEE Transactions on Pattern Analysis and Machine Intelligence*, 2024. [6](#)
- [5] Peter Anderson, Qi Wu, Damien Teney, Jake Bruce, Mark Johnson, Niko Sünderhauf, Ian Reid, Stephen Gould, and Anton van den Hengel. Vision-and-language navigation: Interpreting visually-grounded navigation instructions in real environments. In *Proceedings of the IEEE Conference on Computer Vision and Pattern Recognition*, pages 3674–3683, 2018. [1](#), [2](#), [5](#)
- [6] Peter Anderson, Ayush Shrivastava, Devi Parikh, Dhruv Batra, and Stefan Lee. Chasing ghosts: Instruction following as bayesian state tracking. *Advances in neural information processing systems*, 32, 2019. [2](#)
- [7] Angel Chang, Angela Dai, Thomas Funkhouser, Maciej Halber, Matthias Niebner, Manolis Savva, Shuran Song, Andy Zeng, and Yinda Zhang. Matterport3d: Learning from rgb-d data in indoor environments. In *2017 International Conference on 3D Vision (3DV)*, pages 667–676. IEEE, 2017. [2](#)
- [8] Jinyu Chen, Chen Gao, Erli Meng, Qiong Zhang, and Si Liu. Reinforced structured state-evolution for vision-language navigation. In *Proceedings of the IEEE/CVF Conference on Computer Vision and Pattern Recognition*, pages 15450–15459, 2022. [2](#), [3](#), [6](#)
- [9] Jiaqi Chen, Bingqian Lin, Ran Xu, Zhenhua Chai, Xiaodan Liang, and Kwan-Yee K Wong. Mapgpt: Map-guided prompting with adaptive path planning for vision-and-language navigation. *arXiv preprint arXiv:2401.07314*, 2024. [2](#)
- [10] Kevin Chen, Junshen K Chen, Jo Chuang, Marynel Vázquez, and Silvio Savarese. Topological planning with transformers for vision-and-language navigation. In *Proceedings of the IEEE/CVF Conference on Computer Vision and Pattern Recognition*, pages 11276–11286, 2021. [2](#)
- [11] Peihao Chen, Dongyu Ji, Kunyang Lin, Runhao Zeng, Thomas H Li, Mingkui Tan, and Chuang Gan. Weakly-supervised multi-granularity map learning for vision-and-language navigation. *arXiv preprint arXiv:2210.07506*, 2022. [6](#)
- [12] Shizhe Chen, Pierre-Louis Guhur, Cordelia Schmid, and Ivan Laptev. History aware multimodal transformer for vision-and-language navigation. *Advances in Neural Information Processing Systems*, 34:5834–5847, 2021. [1](#), [2](#), [3](#), [6](#), [8](#)
- [13] Shizhe Chen, Pierre-Louis Guhur, Makarand Tapaswi, Cordelia Schmid, and Ivan Laptev. Think global, act local: Dual-scale graph transformer for vision-and-language navigation. In *Proceedings of the IEEE/CVF Conference on Computer Vision and Pattern Recognition*, pages 16537–16547, 2022. [1](#), [2](#), [5](#), [6](#)
- [14] Shizhe Chen, Pierre-Louis Guhur, Makarand Tapaswi, Cordelia Schmid, and Ivan Laptev. Learning from unlabeled 3d environments for vision-and-language navigation. In *European Conference on Computer Vision*, pages 638–655. Springer, 2022. [3](#)
- [15] Wenhao Cheng, Xingping Dong, Salman Khan, and Jianbing Shen. Learning disentanglement with decoupled labels for vision-language navigation. In *European Conference on Computer Vision*, pages 309–329. Springer, 2022. [2](#)
- [16] Yibo Cui, Liang Xie, Yakun Zhang, Meishan Zhang, Ye Yan, and Erwei Yin. Grounded entity-landmark adaptive pre-training for vision-and-language navigation. In *Proceedings of the IEEE/CVF international conference on computer vision*, pages 12043–12053, 2023. [2](#)
- [17] Zhiwei Deng, Karthik Narasimhan, and Olga Russakovsky. Evolving graphical planner: Contextual global planning for vision-and-language navigation. *Advances in Neural Information Processing Systems*, 33:20660–20672, 2020. [2](#)
- [18] Daniel Fried, Ronghang Hu, Volkan Cirik, Anna Rohrbach, Jacob Andreas, Louis-Philippe Morency, Taylor Berg-Kirkpatrick, Kate Saenko, Dan Klein, and Trevor Darrell. Speaker-follower models for vision-and-language navigation. In *Advances in Neural Information Processing Systems*, pages 3314–3325, 2018. [2](#), [3](#)
- [19] Tsu-Jui Fu, Xin Eric Wang, Matthew F Peterson, Scott T Grafton, Miguel P Eckstein, and William Yang Wang. Counterfactual vision-and-language navigation via adversarial path sampler. In *European Conference on Computer Vision*, pages 71–86. Springer, 2020. [2](#)
- [20] Chen Gao, Xingyu Peng, Mi Yan, He Wang, Lirong Yang, Haibing Ren, Hongsheng Li, and Si Liu. Adaptive zone-aware hierarchical planner for vision-language navigation. In *Proceedings of the IEEE/CVF conference on computer vision and pattern recognition*, pages 14911–14920, 2023. [2](#)
- [21] Pierre-Louis Guhur, Makarand Tapaswi, Shizhe Chen, Ivan Laptev, and Cordelia Schmid. Airbert: In-domain pretraining for vision-and-language navigation. In *Proceedings of the IEEE/CVF International Conference on Computer Vision*, pages 1634–1643, 2021. [2](#)
- [22] Daya Guo, Dejian Yang, Haowei Zhang, Junxiao Song, Ruoyu Zhang, Runxin Xu, Qihao Zhu, Shirong Ma, Peiyi Wang, Xiao Bi, et al. Deepseek-r1: Incentivizing reasoning capability in llms via reinforcement learning. *arXiv preprint arXiv:2501.12948*, 2025. [1](#), [3](#), [7](#)

- [23] Weituo Hao, Chunyuan Li, Xiujun Li, Lawrence Carin, and Jianfeng Gao. Towards learning a generic agent for vision-and-language navigation via pre-training. In *Proceedings of the IEEE/CVF Conference on Computer Vision and Pattern Recognition*, pages 13137–13146, 2020. 2
- [24] Weituo Hao, Chunyuan Li, Xiujun Li, Lawrence Carin, and Jianfeng Gao. Towards learning a generic agent for vision-and-language navigation via pre-training. In *Proceedings of the IEEE/CVF conference on computer vision and pattern recognition*, pages 13137–13146, 2020. 2
- [25] Keji He, Chenyang Si, Zhihe Lu, Yan Huang, Liang Wang, and Xinchao Wang. Frequency-enhanced data augmentation for vision-and-language navigation. *Advances in neural information processing systems*, 36:4351–4364, 2023. 3
- [26] Yicong Hong, Cristian Rodriguez, Yuankai Qi, Qi Wu, and Stephen Gould. Language and visual entity relationship graph for agent navigation. *Advances in Neural Information Processing Systems*, 33, 2020. 2
- [27] Yicong Hong, Cristian Rodriguez-Opazo, Qi Wu, and Stephen Gould. Sub-instruction aware vision-and-language navigation. *arXiv preprint arXiv:2004.02707*, 2020. 2
- [28] Yicong Hong, Qi Wu, Yuankai Qi, Cristian Rodriguez-Opazo, and Stephen Gould. A recurrent vision-and-language bert for navigation. In *Proceedings of the IEEE/CVF Conference on Computer Vision and Pattern Recognition (CVPR)*, pages 1643–1653, 2021. 2, 6
- [29] Yicong Hong, Zun Wang, Qi Wu, and Stephen Gould. Bridging the gap between learning in discrete and continuous environments for vision-and-language navigation. In *Proceedings of the IEEE/CVF Conference on Computer Vision and Pattern Recognition*, pages 15439–15449, 2022. 6
- [30] Yicong Hong, Yang Zhou, Ruiyi Zhang, Franck Dornoncourt, Trung Bui, Stephen Gould, and Hao Tan. Learning navigational visual representations with semantic map supervision. In *Proceedings of the IEEE/CVF International Conference on Computer Vision*, pages 3055–3067, 2023. 2
- [31] Ronghang Hu, Daniel Fried, Anna Rohrbach, Dan Klein, Trevor Darrell, and Kate Saenko. Are you looking? grounding to multiple modalities in vision-and-language navigation. *arXiv preprint arXiv:1906.00347*, 2019. 2
- [32] Haoshuo Huang, Vihan Jain, Harsh Mehta, Jason Baldrige, and Eugene Ie. Multi-modal discriminative model for vision-and-language navigation. *arXiv preprint arXiv:1905.13358*, 2019. 3
- [33] Haoshuo Huang, Vihan Jain, Harsh Mehta, Alexander Ku, Gabriel Magalhaes, Jason Baldrige, and Eugene Ie. Transferable representation learning in vision-and-language navigation. In *Proceedings of the IEEE/CVF international conference on computer vision*, pages 7404–7413, 2019. 2
- [34] Jingyang Huo, Qiang Sun, Boyan Jiang, Haitao Lin, and Yanwei Fu. Geovln: Learning geometry-enhanced visual representation with slot attention for vision-and-language navigation. In *Proceedings of the IEEE/CVF conference on computer vision and pattern recognition*, pages 23212–23221, 2023. 2
- [35] Minyoung Hwang, Jaeyeon Jeong, Minsoo Kim, Yoonseon Oh, and Songhwai Oh. Meta-explore: Exploratory hierarchical vision-and-language navigation using scene object spectrum grounding. In *Proceedings of the IEEE/CVF Conference on Computer Vision and Pattern Recognition*, pages 6683–6693, 2023. 2
- [36] Vihan Jain, Gabriel Magalhaes, Alexander Ku, Ashish Vaswani, Eugene Ie, and Jason Baldrige. Stay on the path: Instruction fidelity in vision-and-language navigation. In *Proceedings of the 57th Annual Meeting of the Association for Computational Linguistics*, pages 1862–1872, 2019. 2
- [37] Aishwarya Kamath, Peter Anderson, Su Wang, Jing Yu Koh, Alexander Ku, Austin Waters, Yinfei Yang, Jason Baldrige, and Zarana Parekh. A new path: Scaling vision-and-language navigation with synthetic instructions and imitation learning. In *Proceedings of the IEEE/CVF conference on computer vision and pattern recognition*, pages 10813–10823, 2023. 3
- [38] Liyiming Ke, Xiujun Li, Yonatan Bisk, Ari Holtzman, Zhe Gan, Jingjing Liu, Jianfeng Gao, Yejin Choi, and Siddhartha Srinivasa. Tactical rewind: Self-correction via backtracking in vision-and-language navigation. In *Proceedings of the IEEE/CVF conference on computer vision and pattern recognition*, pages 6741–6749, 2019. 2
- [39] Jing Yu Koh, Harsh Agrawal, Dhruv Batra, Richard Tucker, Austin Waters, Honglak Lee, Yinfei Yang, Jason Baldrige, and Peter Anderson. Simple and effective synthesis of indoor 3d scenes. *arXiv preprint arXiv:2204.02960*, 2022. 3
- [40] Xianghao Kong, Jinyu Chen, Wenguan Wang, Hang Su, Xiaolin Hu, Yi Yang, and Si Liu. Controllable navigation instruction generation with chain of thought prompting. *arXiv preprint arXiv:2407.07433*, 2024. 3
- [41] Jacob Krantz and Stefan Lee. Sim-2-sim transfer for vision-and-language navigation in continuous environments. In *European Conference on Computer Vision*, pages 588–603. Springer, 2022. 6
- [42] Jacob Krantz, Erik Wijmans, Arjun Majumdar, Dhruv Batra, and Stefan Lee. Beyond the nav-graph: Vision-and-language navigation in continuous environments. In *Computer Vision–ECCV 2020: 16th European Conference, Glasgow, UK, August 23–28, 2020, Proceedings, Part XXVIII 16*, pages 104–120. Springer, 2020. 2, 5
- [43] Alexander Ku, Peter Anderson, Roma Patel, Eugene Ie, and Jason Baldrige. Room-across-room: Multilingual vision-and-language navigation with dense spatiotemporal grounding. In *Proceedings of the 2020 Conference on Empirical Methods in Natural Language Processing (EMNLP)*, pages 4392–4412, 2020. 2
- [44] Shuhei Kurita and Kyunghyun Cho. Generative language-grounded policy in vision-and-language navigation with bayes’ rule. *arXiv preprint arXiv:2009.07783*, 2020. 2
- [45] Jialu Li and Mohit Bansal. Panogen: Text-conditioned panoramic environment generation for vision-and-language navigation. *arXiv preprint arXiv:2305.19195*, 2023. 3
- [46] Jialu Li, Hao Tan, and Mohit Bansal. Improving cross-modal alignment in vision language navigation via syntactic information. *arXiv preprint arXiv:2104.09580*, 2021. 2

- [47] Jialu Li, Hao Tan, and Mohit Bansal. Envedit: Environment editing for vision-and-language navigation. In *Proceedings of the IEEE/CVF Conference on Computer Vision and Pattern Recognition*, pages 15407–15417, 2022. 3
- [48] Mingxiao Li, Zehao Wang, Tinne Tuytelaars, and Marie-Francine Moens. Layout-aware dreamer for embodied visual referring expression grounding. In *Proceedings of the AAAI Conference on Artificial Intelligence*, pages 1386–1395, 2023. 2
- [49] Xiujun Li, Chunyuan Li, Qiaolin Xia, Yonatan Bisk, Asli Celikyilmaz, Jianfeng Gao, Noah Smith, and Yejin Choi. Robust navigation with language pretraining and stochastic sampling. *arXiv preprint arXiv:1909.02244*, 2019. 2
- [50] Xiangyang Li, Zihan Wang, Jiahao Yang, Yaowei Wang, and Shuqiang Jiang. Kerm: Knowledge enhanced reasoning for vision-and-language navigation. In *Proceedings of the IEEE/CVF Conference on Computer Vision and Pattern Recognition*, pages 2583–2592, 2023. 2, 6
- [51] Xiwen Liang, Fengda Zhu, Lingling Li, Hang Xu, and Xiaodan Liang. Visual-language navigation pretraining via prompt-based environmental self-exploration. *arXiv preprint arXiv:2203.04006*, 2022. 3
- [52] Xiwen Liang, Fengda Zhu, Yi Zhu, Bingqian Lin, Bing Wang, and Xiaodan Liang. Contrastive instruction-trajectory learning for vision-language navigation. In *Proceedings of the AAAI Conference on Artificial Intelligence*, pages 1592–1600, 2022. 2
- [53] Bingqian Lin, Yi Zhu, Yanxin Long, Xiaodan Liang, Qixiang Ye, and Liang Lin. Adversarial reinforced instruction attacker for robust vision-language navigation. *IEEE Transactions on Pattern Analysis and Machine Intelligence*, 44(10):7175–7189, 2021. 2
- [54] Bingqian Lin, Yi Zhu, Zicong Chen, Xiwen Liang, Jianzhuang Liu, and Xiaodan Liang. Adapt: Vision-language navigation with modality-aligned action prompts. In *Proceedings of the IEEE/CVF Conference on Computer Vision and Pattern Recognition*, pages 15396–15406, 2022. 2
- [55] Bingqian Lin, Yi Zhu, Xiaodan Liang, Liang Lin, and Jianzhuang Liu. Actional atomic-concept learning for demystifying vision-language navigation. In *Proceedings of the AAAI Conference on Artificial Intelligence*, pages 1568–1576, 2023. 2
- [56] Bingqian Lin, Yunshuang Nie, Ziming Wei, Yi Zhu, Hang Xu, Shikui Ma, Jianzhuang Liu, and Xiaodan Liang. Correctable landmark discovery via large models for vision-language navigation. *IEEE Transactions on Pattern Analysis and Machine Intelligence*, 46(12):8534–8548, 2024. 2
- [57] Chuang Lin, Yi Jiang, Jianfei Cai, Lizhen Qu, Gholamreza Haffari, and Zehuan Yuan. Multimodal transformer with variable-length memory for vision-and-language navigation. In *Computer Vision—ECCV 2022: 17th European Conference, Tel Aviv, Israel, October 23–27, 2022, Proceedings, Part XXXVI*, pages 380–397. Springer, 2022. 2
- [58] Kuniyang Lin, Peihao Chen, Diwei Huang, Thomas H Li, Mingkui Tan, and Chuang Gan. Learning vision-and-language navigation from youtube videos. In *Proceedings of the IEEE/CVF International Conference on Computer Vision*, pages 8317–8326, 2023. 3
- [59] Xiangru Lin, Guanbin Li, and Yizhou Yu. Scene-intuitive agent for remote embodied visual grounding. In *Proceedings of the IEEE/CVF Conference on Computer Vision and Pattern Recognition*, pages 7036–7045, 2021. 2
- [60] Chong Liu, Fengda Zhu, Xiaojun Chang, Xiaodan Liang, Zongyuan Ge, and Yi-Dong Shen. Vision-language navigation with random environmental mixup. In *Proceedings of the IEEE/CVF International Conference on Computer Vision*, pages 1644–1654, 2021. 3
- [61] Rui Liu, Xiaohan Wang, Wenguan Wang, and Yi Yang. Bird’s-eye-view scene graph for vision-language navigation. In *Proceedings of the IEEE/CVF International Conference on Computer Vision*, pages 10968–10980, 2023. 2
- [62] Rui Liu, Wenguan Wang, and Yi Yang. Volumetric environment representation for vision-language navigation. In *Proceedings of the IEEE/CVF Conference on Computer Vision and Pattern Recognition*, pages 16317–16328, 2024. 2, 6
- [63] Zichen Liu, Changyu Chen, Wenjun Li, Penghui Qi, Tianyu Pang, Chao Du, Wee Sun Lee, and Min Lin. Understanding r1-zero-like training: A critical perspective. *arXiv preprint arXiv:2503.20783*, 2025. 3, 7, 1
- [64] Yuxing Long, Xiaoqi Li, Wenzhe Cai, and Hao Dong. Discuss before moving: Visual language navigation via multi-expert discussions. In *2024 IEEE International Conference on Robotics and Automation (ICRA)*, pages 17380–17387. IEEE, 2024. 2
- [65] Chih-Yao Ma, Jiasen Lu, Zuxuan Wu, Ghassan AlRegib, Zolt Kira, Richard Socher, and Caiming Xiong. Self-monitoring navigation agent via auxiliary progress estimation. In *Proceedings of the International Conference on Learning Representations (ICLR)*, 2019. 2
- [66] Arjun Majumdar, Ayush Shrivastava, Stefan Lee, Peter Anderson, Devi Parikh, and Dhruv Batra. Improving vision-and-language navigation with image-text pairs from the web. In *Proceedings of the European Conference on Computer Vision*, 2020. 2
- [67] Abhinav Moudgil, Arjun Majumdar, Harsh Agrawal, Stefan Lee, and Dhruv Batra. Soat: A scene-and object-aware transformer for vision-and-language navigation. *Advances in Neural Information Processing Systems*, 34:7357–7367, 2021. 2
- [68] Bowen Pan, Rameswar Panda, SouYoung Jin, Rogerio Feris, Aude Oliva, Phillip Isola, and Yoon Kim. Langnav: Language as a perceptual representation for navigation. *arXiv preprint arXiv:2310.07889*, 2023. 2
- [69] Amin Parvaneh, Ehsan Abbasnejad, Damien Teney, Javen Qinfeng Shi, and Anton Van den Hengel. Counterfactual vision-and-language navigation: Unravelling the unseen. *Advances in neural information processing systems*, 33:5296–5307, 2020. 2
- [70] Yuankai Qi, Zizheng Pan, Shengping Zhang, Anton van den Hengel, and Qi Wu. Object-and-action aware model for visual language navigation. In *European Conference on Computer Vision*, 2020. 2

- [71] Yuankai Qi, Qi Wu, Peter Anderson, Xin Wang, William Yang Wang, Chunhua Shen, and Anton van den Hengel. Reverie: Remote embodied visual referring expression in real indoor environments. In *Proceedings of the IEEE/CVF Conference on Computer Vision and Pattern Recognition*, pages 9982–9991, 2020. 2, 5
- [72] Yuankai Qi, Zizheng Pan, Yicong Hong, Ming-Hsuan Yang, Anton van den Hengel, and Qi Wu. The road to know-where: An object-and-room informed sequential bert for indoor vision-language navigation. In *Proceedings of the IEEE/CVF International Conference on Computer Vision*, pages 1655–1664, 2021. 2
- [73] Yanyuan Qiao, Yuankai Qi, Yicong Hong, Zheng Yu, Peng Wang, and Qi Wu. Hop: History-and-order aware pre-training for vision-and-language navigation. In *Proceedings of the IEEE/CVF Conference on Computer Vision and Pattern Recognition*, pages 15418–15427, 2022. 2
- [74] Yanyuan Qiao, Yuankai Qi, Yicong Hong, Zheng Yu, Peng Wang, and Qi Wu. Hop+: History-enhanced and order-aware pre-training for vision-and-language navigation. *IEEE Transactions on Pattern Analysis and Machine Intelligence*, 2023. 6
- [75] Yanyuan Qiao, Yuankai Qi, Zheng Yu, Jing Liu, and Qi Wu. March in chat: Interactive prompting for remote embodied referring expression. In *Proceedings of the IEEE/CVF International Conference on Computer Vision*, pages 15758–15767, 2023. 2
- [76] Yanyuan Qiao, Qianyi Liu, Jiajun Liu, Jing Liu, and Qi Wu. Llm as copilot for coarse-grained vision-and-language navigation. In *European Conference on Computer Vision*, pages 459–476, 2024. 2
- [77] Sonia Raychaudhuri, Saim Wani, Shivansh Patel, Unnat Jain, and Angel X Chang. Language-aligned waypoint (law) supervision for vision-and-language navigation in continuous environments. *arXiv preprint arXiv:2109.15207*, 2021. 6
- [78] Manolis Savva, Abhishek Kadian, Oleksandr Maksymets, Yili Zhao, Erik Wijmans, Bhavana Jain, Julian Straub, Jia Liu, Vladlen Koltun, Jitendra Malik, et al. Habitat: A platform for embodied ai research. In *Proceedings of the IEEE/CVF International Conference on Computer Vision*, pages 9339–9347, 2019. 5
- [79] John Schulman, Filip Wolski, Prafulla Dhariwal, Alec Radford, and Oleg Klimov. Proximal policy optimization algorithms. *arXiv preprint arXiv:1707.06347*, 2017. 4, 5
- [80] Hao Tan, Licheng Yu, and Mohit Bansal. Learning to navigate unseen environments: Back translation with environmental dropout. In *Proceedings of NAACL-HLT*, pages 2610–2621, 2019. 3
- [81] Hanqing Wang, Wenguan Wang, Tianmin Shu, Wei Liang, and Jianbing Shen. Active visual information gathering for vision-language navigation. In *European Conference on Computer Vision*, pages 307–322. Springer, 2020. 2
- [82] Hu Wang, Qi Wu, and Chunhua Shen. Soft expert reward learning for vision-and-language navigation. In *European Conference on Computer Vision*, pages 126–141. Springer, 2020. 2, 3, 6
- [83] Hanqing Wang, Wenguan Wang, Wei Liang, Caiming Xiong, and Jianbing Shen. Structured scene memory for vision-language navigation. In *Proceedings of the IEEE/CVF Conference on Computer Vision and Pattern Recognition*, pages 8455–8464, 2021. 2
- [84] Hanqing Wang, Wei Liang, Jianbing Shen, Luc Van Gool, and Wenguan Wang. Counterfactual cycle-consistent learning for instruction following and generation in vision-language navigation. In *Proceedings of the IEEE/CVF conference on computer vision and pattern recognition*, pages 15471–15481, 2022. 2
- [85] Liuyi Wang, Zongtao He, Jiagui Tang, Ronghao Dang, Naijia Wang, Chengju Liu, and Qijun Chen. A dual semantic-aware recurrent global-adaptive network for vision-and-language navigation. *arXiv preprint arXiv:2305.03602*, 2023. 2
- [86] Liuyi Wang, Zongtao He, Ronghao Dang, Mengjiao Shen, Chengju Liu, and Qijun Chen. Vision-and-language navigation via causal learning. In *The IEEE/CVF Conference on Computer Vision and Pattern Recognition (CVPR)*, 2024. 2, 6
- [87] Liuyi Wang, Zongtao He, Mengjiao Shen, Jingwei Yang, Chengju Liu, and Qijun Chen. Magic: Meta-ability guided interactive chain-of-distillation for effective-and-efficient vision-and-language navigation. *arXiv preprint arXiv:2406.17960*, 2024. 6
- [88] Su Wang, Ceslee Montgomery, Jordi Orbay, Vighnesh Birodkar, Aleksandra Faust, Izzeddin Gur, Natasha Jaques, Austin Waters, Jason Baldrige, and Peter Anderson. Less is more: Generating grounded navigation instructions from landmarks. In *Proceedings of the IEEE/CVF Conference on Computer Vision and Pattern Recognition*, pages 15428–15438, 2022. 3
- [89] Xin Wang, Wenhan Xiong, Hongmin Wang, and William Yang Wang. Look before you leap: Bridging model-free and model-based reinforcement learning for planned-ahead vision-and-language navigation. In *Proceedings of the European Conference on Computer Vision (ECCV)*, pages 37–53, 2018. 2
- [90] Xin Wang, Qiuyuan Huang, Asli Celikyilmaz, Jianfeng Gao, Dinghan Shen, Yuan-Fang Wang, William Yang Wang, and Lei Zhang. Reinforced cross-modal matching and self-supervised imitation learning for vision-language navigation. In *Proceedings of the IEEE Conference on Computer Vision and Pattern Recognition*, pages 6629–6638, 2019. 1, 2, 3, 6
- [91] Xiaohan Wang, Wenguan Wang, Jiayi Shao, and Yi Yang. Lana: A language-capable navigator for instruction following and generation. In *Proceedings of the IEEE/CVF Conference on Computer Vision and Pattern Recognition*, pages 19048–19058, 2023. 2, 6
- [92] Xin Eric Wang, Vihan Jain, Eugene Ie, William Yang Wang, Zornitsa Kozareva, and Sujith Ravi. Environment-agnostic multitask learning for natural language grounded navigation. In *Computer Vision—ECCV 2020: 16th European Conference, Glasgow, UK, August 23–28, 2020, Proceedings, Part XXIV 16*, pages 413–430. Springer, 2020. 2

- [93] Zun Wang, Jialu Li, Yicong Hong, Yi Wang, Qi Wu, Mohit Bansal, Stephen Gould, Hao Tan, and Yu Qiao. Scaling data generation in vision-and-language navigation. In *Proceedings of the IEEE/CVF International Conference on Computer Vision (ICCV)*, pages 12009–12020, 2023. 3, 5, 6
- [94] Zihan Wang, Xiangyang Li, Jiahao Yang, Yeqi Liu, and Shuqiang Jiang. Gridmm: Grid memory map for vision-and-language navigation. In *Proceedings of the IEEE/CVF International Conference on Computer Vision*, pages 15625–15636, 2023. 2, 6
- [95] Zun Wang, Jialu Li, Yicong Hong, Songze Li, Kunchang Li, Shoubin Yu, Yi Wang, Yu Qiao, Yali Wang, Mohit Bansal, et al. Bootstrapping language-guided navigation learning with self-refining data flywheel. *arXiv preprint arXiv:2412.08467*, 2024. 3
- [96] Peiran Xu, Xicheng Gong, and Yadong Mu. Navq: Learning a q-model for foresighted vision-and-language navigation. In *Proceedings of the IEEE/CVF International Conference on Computer Vision*, pages 6327–6341, 2025. 6
- [97] Jiwen Zhang, Jianqing Fan, Jiajie Peng, et al. Curriculum learning for vision-and-language navigation. *Advances in Neural Information Processing Systems*, 34:13328–13339, 2021. 2
- [98] Siqi Zhang, Yanyuan Qiao, Qunbo Wang, Zike Yan, Qi Wu, Zhihua Wei, and Jing Liu. Cosmo: Combination of selective memorization for low-cost vision-and-language navigation. *arXiv preprint arXiv:2503.24065*, 2025. 6
- [99] Weixia Zhang, Chao Ma, Qi Wu, and Xiaokang Yang. Language-guided navigation via cross-modal grounding and alternate adversarial learning. *IEEE Transactions on Circuits and Systems for Video Technology*, 31(9):3469–3481, 2020. 2
- [100] Yue Zhang and Parisa Kordjamshidi. Vln-trans: Translator for the vision and language navigation agent. *arXiv preprint arXiv:2302.09230*, 2023. 2
- [101] Yubo Zhang, Hao Tan, and Mohit Bansal. Diagnosing the environment bias in vision-and-language navigation. *arXiv preprint arXiv:2005.03086*, 2020. 2
- [102] Yuzhong Zhao, Yue Liu, Junpeng Liu, Jingye Chen, Xun Wu, Yaru Hao, Tengchao Lv, Shaohan Huang, Lei Cui, Qixiang Ye, et al. Geometric-mean policy optimization. *arXiv preprint arXiv:2507.20673*, 2025. 7, 1
- [103] Chujie Zheng, Shixuan Liu, Mingze Li, Xiong-Hui Chen, Bowen Yu, Chang Gao, Kai Dang, Yuqiong Liu, Rui Men, An Yang, et al. Group sequence policy optimization. *arXiv preprint arXiv:2507.18071*, 2025. 7, 1
- [104] Duo Zheng, Shijia Huang, Lin Zhao, Yiwu Zhong, and Liwei Wang. Towards learning a generalist model for embodied navigation. In *Proceedings of the IEEE/CVF Conference on Computer Vision and Pattern Recognition*, pages 13624–13634, 2024. 2, 6
- [105] Gengze Zhou, Yicong Hong, and Qi Wu. Navgpt: Explicit reasoning in vision-and-language navigation with large language models. *arXiv preprint arXiv:2305.16986*, 2023.
- [106] Gengze Zhou, Yicong Hong, Zun Wang, Xin Eric Wang, and Qi Wu. Navgpt-2: Unleashing navigational reasoning capability for large vision-language models. In *European Conference on Computer Vision*, pages 260–278, 2024. 2, 6
- [107] Fengda Zhu, Yi Zhu, Xiaojun Chang, and Xiaodan Liang. Vision-language navigation with self-supervised auxiliary reasoning tasks. In *Proceedings of the IEEE/CVF Conference on Computer Vision and Pattern Recognition*, pages 10012–10022, 2020. 2
- [108] Fengda Zhu, Xiwen Liang, Yi Zhu, Qizhi Yu, Xiaojun Chang, and Xiaodan Liang. Soon: Scenario oriented object navigation with graph-based exploration. In *Proceedings of the IEEE/CVF Conference on Computer Vision and Pattern Recognition*, pages 12689–12699, 2021. 2
- [109] Wang Zhu, Hexiang Hu, Jiacheng Chen, Zhiwei Deng, Vihan Jain, Eugene Ie, and Fei Sha. Babywalk: Going farther in vision-and-language navigation by taking baby steps. *arXiv preprint arXiv:2005.04625*, 2020. 2

Trajectory-Diversity-Driven Robust Vision-and-Language Navigation

Supplementary Material

6. GRPO Variants Implementation

We provide detailed formulations of the group-based policy optimization variants evaluated in our experiments. All variants share the same trajectory sampling strategy but differ in advantage estimation and policy update mechanisms. **GRPO** [22]. Uses group-wise advantage normalization with both variance and length normalization:

$$\hat{A}_k = \frac{r_k - \text{mean}(\{r_1, \dots, r_K\})}{\text{std}(\{r_1, \dots, r_K\})} \quad (12)$$

The policy objective aggregates with length normalization:

$$\mathcal{J}_{\text{GRPO}} = \mathbb{E} \left[\frac{1}{K} \sum_{k=1}^K \frac{1}{|\tau_k|} \sum_{t=1}^{|\tau_k|} \rho_{k,t} \hat{A}_k \right] \quad (13)$$

where $\rho_{k,t}(\theta) = \pi_\theta(a_{k,t}|s_{k,t})/\pi_{\text{old}}(a_{k,t}|s_{k,t})$ with clipping omitted for brevity. Variance normalization ensures consistent gradient scales across batches, while the $1/|\tau_k|$ term computes per-token average gradients. Token-level importance sampling applies independent ratio clipping at each time step.

GSPO [103]. Shifts importance sampling to sequence level. The sequence-level importance ratio is:

$$s_k(\theta) = \exp \left(\frac{1}{|\tau_k|} \sum_{t=1}^{|\tau_k|} \log \frac{\pi_\theta(a_{k,t}|s_{k,t})}{\pi_{\text{old}}(a_{k,t}|s_{k,t})} \right) \quad (14)$$

The objective applies trajectory-level clipping:

$$\mathcal{J}_{\text{GSPO}} = \mathbb{E} \left[\frac{1}{K} \sum_{k=1}^K s_k \hat{A}_k \right] \quad (15)$$

The sequence-level importance ratio s_k aggregates token probabilities across the entire trajectory before clipping. This can be overly aggressive as it discards all tokens once triggered.

GMPO [102]. Replaces arithmetic mean with geometric mean for token-level rewards, computed in log space for numerical stability. The objective is:

$$\mathcal{J}_{\text{GMPO}} = \mathbb{E} \left[\frac{1}{K} \sum_{k=1}^K \text{sgn}(\hat{A}_k) \cdot \left(\prod_{t=1}^{|\tau_k|} |\rho_{k,t} \hat{A}_k| \right)^{\frac{1}{|\tau_k|}} \right] \quad (16)$$

where clipping is omitted for brevity. The geometric mean inherently suppresses outliers, yielding more stable importance sampling ratios. GMPO employs token-level clipping with an exponential range ($e^{-\epsilon}, e^\epsilon$) that is wider than GRPO’s linear range ($1 - \epsilon, 1 + \epsilon$).

7. Dr.GRPO for VLN

7.1. Background: Standard GRPO vs. Dr.GRPO

Standard GRPO [22], designed for language model alignment, applies two normalization terms to the advantage estimation:

$$\hat{A}_k^{\text{GRPO}} = \frac{1}{|\tau_k|} \cdot \frac{r_k - \text{mean}(\{r_1, \dots, r_K\})}{\text{std}(\{r_1, \dots, r_K\})} \quad (17)$$

where $|\tau_k|$ is the trajectory length and $\text{std}(\{r_1, \dots, r_K\})$ is the standard deviation of rewards across K rollouts. While these normalizations are appropriate for open-ended text generation, they introduce optimization biases detrimental to navigation learning.

Dr.GRPO [63] eliminates both normalizations through unbiased advantage estimation:

$$\hat{A}_k = r_k - \text{mean}(\{r_1, \dots, r_K\}) \quad (18)$$

and aggregates gradients without normalization:

$$\mathcal{J}_{\text{Dr.GRPO}} = \mathbb{E} \left[\frac{1}{K} \sum_{k=1}^K \sum_{t=1}^{|\tau_k|} \rho_{k,t} \hat{A}_k \right] \quad (19)$$

This recovers the theoretically grounded Monte Carlo policy gradient with an unbiased baseline.

7.2. Why Standard GRPO Fails for VLN

The two normalization terms in standard GRPO create specific problems for embodied navigation tasks:

Length Normalization Bias. The $1/|\tau_k|$ term divides the advantage by trajectory length to treat each token equally in language model training. However, in VLN, trajectory length naturally reflects scene complexity and navigation difficulty—longer paths may traverse larger buildings or require more precise localization. Empirically, R2R trajectories range from 5 to 15+ meters with an average of approximately 10 meters, exhibiting substantial variance. This creates asymmetric gradient updates:

- **Correct short paths** receive amplified gradients ($\propto 1/\text{short}$), encouraging shortcuts even when inappropriate.
- **Incorrect long paths** receive diluted penalties ($\propto 1/\text{long}$), failing to discourage wandering behavior when the agent is lost.

Variance Normalization Bias. The $1/\text{std}(\{r_1, \dots, r_K\})$ term amplifies gradients for instructions where all K rollouts yield similar outcomes (low variance). This assigns disproportionate weight to:

Algorithm 1 Dr.GRPO for VLN

Require: Pretrained policy π_{ref} , instruction set \mathcal{D} , Batch size B , group size K , hyperparameters α, δ, β

```
1: Initialize  $\pi_\theta \leftarrow \pi_{\text{ref}}, \mathcal{B}_{\text{hard}} \leftarrow \emptyset$ 
2: for iteration = 1, 2, ... do
3:   Sample  $\{W_i\}_{i=1}^B \sim \mathcal{D}; \pi_{\text{old}} \leftarrow \pi_\theta$ 
4:   for each  $W_i$  do
5:     for  $k = 1$  to  $K$  do
6:       Sample  $\tau_k \sim \pi_{\text{old}}(\cdot | W_i)$ ; compute  $r_k$  (Eq. 8)
7:     end for
8:     Compute  $\hat{A}_k = r_k - \frac{1}{K} \sum_{j=1}^K r_j$  for all  $k$ 
9:     if  $\sum_{k=1}^K \mathbb{1}(d_k < \epsilon) = 0$  then
10:       $\mathcal{B}_{\text{hard}} \leftarrow \mathcal{B}_{\text{hard}} \cup \{W_i\}$ 
11:    end if
12:  end for
13:  Update  $\pi_\theta$  via gradient ascent (Eq. 5)
14:  if  $|\mathcal{B}_{\text{hard}}| \geq M$  then
15:    SFT on  $\mathcal{B}_{\text{hard}}$  (Eq. 11);  $\mathcal{B}_{\text{hard}} \leftarrow \emptyset$ 
16:  end if
17: end for
18: return  $\pi_\theta$ 
```

- **‘Easy’ instructions** where all rollouts succeed (low learning value).
- **‘Hard’ instructions** where all rollouts fail (no positive signal to exploit).

Both scenarios provide minimal actionable gradients, yet receive higher weight than instructions with mixed success/failure (high learning value). For VLN, where learning should prioritize instructions that distinguish successful from failed behaviors, this variance-based weighting is counterproductive.

By removing both normalizations, Dr.GRPO ensures that gradient magnitudes reflect true action importance rather than being artificially modulated by path length or scenario-specific variance, yielding more principled policy updates and improved sample efficiency.

Algorithm 1 presents the complete training procedure.

8. Additional Experiments

8.1. Comparison with More RL Methods

We compare with HAMA [12], a representative value-based RL approach that applies policy gradient optimization with auxiliary value networks for vision-language navigation. We implement HAMA’s training pipeline on ScaleVLN under identical training data and computational budget to ensure fair comparison.

Table 9 demonstrates NavGRPO’s clear advantage over HAMA across all settings. Under standard conditions, NavGRPO achieves +6.53% SPL improvement. Under perturbations, NavGRPO exhibits substantially stronger robust-

Table 9. Comparison with value-based RL method (HAMA) under standard and perturbed settings on R2R Val Unseen. Both methods build upon ScaleVLN baseline.

Method	OSR \uparrow	NE \downarrow	SR \uparrow	SPL \uparrow	Δ SPL
Standard (No Perturbation)					
ScaleVLN + HAMA	83.07	2.65	74.98	66.12	-0.00
ScaleVLN + NavGRPO	89.18	2.19	81.88	72.65	-0.00
Global Perturbation ($p = 0.8$)					
ScaleVLN + HAMA	82.14	2.83	72.01	61.92	-4.20
ScaleVLN + NavGRPO	88.49	2.27	79.95	69.98	-2.67
Early Perturbation (Steps=2)					
ScaleVLN + HAMA	75.24	3.09	67.16	55.15	-10.97
ScaleVLN + NavGRPO	83.85	2.70	76.50	65.10	-7.55

Table 10. Ablation study on path efficiency weight α in R_{path} on R2R Val Unseen split.

α	OSR \uparrow	NE \downarrow	SR \uparrow	SPL \uparrow
0.0	88.64	2.26	81.92	71.48
0.25	89.18	2.19	81.88	72.65
0.5	88.71	2.23	81.34	71.92
1.0	88.23	2.31	80.76	70.85

ness: degrading 1.6 \times less than HAMA under global perturbation and 1.5 \times less under early perturbation.

More revealing is the comparison across learning paradigms. While HAMA improves robustness over imitation learning, degrading roughly half as much as ScaleVLN under global perturbations, it suffers severe success rate collapse under extreme scenarios. HAMA’s success rate drops 7.82% under 2-step early perturbation compared to ScaleVLN’s 3.71% drop, revealing that traditional value-based RL struggles to maintain task completion capability when facing critical early errors.

The performance gap stems from two fundamental differences. First, value-based methods require training critic networks to approximate state values, which suffers from instability in VLN’s high-dimensional action space. Second, traditional RL optimizes trajectories independently using absolute rewards, learning what is “correct.” NavGRPO instead performs group-relative optimization—sampling diverse rollouts per instruction and learning through within-group comparison. This enables distinguishing relative quality among strategies under identical instructions, extracting supervision from both successful and failed trajectories that value-based methods cannot capture when optimizing trajectories in isolation.

Table 11. Ablation study on entropy regularization coefficient β on R2R Val Unseen split.

β	OSR \uparrow	NE \downarrow	SR \uparrow	SPL \uparrow
0.0	88.52	2.27	81.64	72.28
0.01	89.18	2.19	81.88	72.65
0.05	88.73	2.24	81.52	71.84
0.1	88.21	2.32	80.92	70.56

Table 12. Impact of hard case buffer size M on R2R Val Unseen split. All variants substantially outperform Sequential SFT-RL baseline.

Training Strategy	OSR \uparrow	NE \downarrow	SR \uparrow	SPL \uparrow
Sequential SFT-RL	88.95	2.22	81.25	72.08
Ours (M=100)	88.89	2.23	81.64	72.41
Ours (M=200)	89.18	2.19	81.88	72.65
Ours (M=400)	89.02	2.20	81.77	72.53

8.2. Extended Ablation Studies

Effect of Path Efficiency Weight α . Table 10 demonstrates the impact of path efficiency weight α in R_{path} . Without path guidance at $\alpha = 0$, the agent achieves highest success rate but suffers 1.17 SPL degradation due to inefficient detours, revealing the trade-off between task completion and path quality. Our default $\alpha = 0.25$ strikes optimal balance, jointly optimizing both metrics. As α increases, performance degrades monotonically: $\alpha = 1.0$ causes 1.8 SPL and 1.12 SR drops. This pattern reveals a limitation of excessive path efficiency enforcement. When deviations from oracle trajectories are heavily penalized, the agent develops brittle behavior that rigidly follows expected routes. In scenarios requiring adaptive replanning around obstacles or unexpected states, such rigidity leads to navigation failure rather than flexible recovery.

Robustness to Clipping and Entropy Regularization. We examine the sensitivity of our method to the entropy regularization coefficient β , as shown in Table 11. Starting from a well-performing SFT policy, we find that a small amount of entropy regularization with $\beta = 0.01$ slightly improves performance compared to no regularization at $\beta = 0.0$. This can be attributed to the entropy term providing a mild regularization effect that prevents the policy from deviating too aggressively from the initial SFT policy during RL fine-tuning, thereby preserving the beneficial behaviors learned from supervised demonstrations. However, when β is set too high at 0.1, performance degrades significantly. Excessive entropy regularization overly restricts the policy’s ability to explore and deviate from the SFT initialization, limiting the potential improvements that RL can achieve through reward-driven optimization. The relatively small performance gap between $\beta = 0.0$ and $\beta = 0.01$ suggests that our training framework strikes a good balance with-

Table 13. Computational cost comparison between ScaleVLN and NavGRPO on R2R training.

	ScaleVLN	Ours(K=4)	Ours(K=8)
NE \downarrow	2.34	2.28	2.19
SR \uparrow	79.40	80.37	81.88
SPL \uparrow	69.97	71.98	72.65
FLOPs(G)	4.95	4.95	4.95
Batchsize	16	8	8
Rollouts per Sample	2	4	8
Peak GPU Memory(GB) \downarrow	20.274	14.788	28.652
Training Time(min/1k steps) \downarrow	46	51	86

out requiring strong entropy constraints. Regarding the clipping threshold δ , we do not conduct extensive ablation experiments as our training procedure accumulates gradients across all samples within a single rollout before performing a unified policy update. This ensures that the policy update remains on-policy, and the gradient accumulation naturally stabilizes the update magnitude without requiring aggressive clipping. We use the standard value $\delta = 0.2$ throughout our experiments.

Hard Case Buffer Size. Table 12 shows the impact of hard case buffer size M. Performance remains stable across $M \in \{100, 200, 400\}$, with minimal variation in SR and SPL. This robustness stems from two factors: first, hard case updates are triggered only when all K sampled trajectories fail, making the actual update frequency relatively low regardless of buffer size; second, our GRPO training already maintains reasonable coverage of diverse navigation scenarios, reducing reliance on explicit hard case intervention. We include this mechanism primarily as a training stabilizer to prevent catastrophic forgetting on persistently challenging instructions, rather than as a core algorithmic component. We adopt $M = 200$ as a conservative choice that balances memory overhead and potential benefit without introducing additional hyperparameter sensitivity.

9. Computational Cost Analysis

Table 13 presents a comprehensive computational cost comparison between ScaleVLN and NavGRPO on a single NVIDIA A800 GPU. NavGRPO with K=4 demonstrates superior memory efficiency, consuming only 14.788 GB of peak GPU memory compared to ScaleVLN’s 20.274 GB, despite generating twice the number of rollouts per sample. This efficiency stems from our decoupled sampling-training architecture: the sampling phase computes visual feature embeddings and graph representations without maintaining computational graphs, caching only the processed features, while the training phase reconstructs gradients solely through the policy network using these cached representations, thereby eliminating redundant forward passes for visual feature computation and substantially reducing the

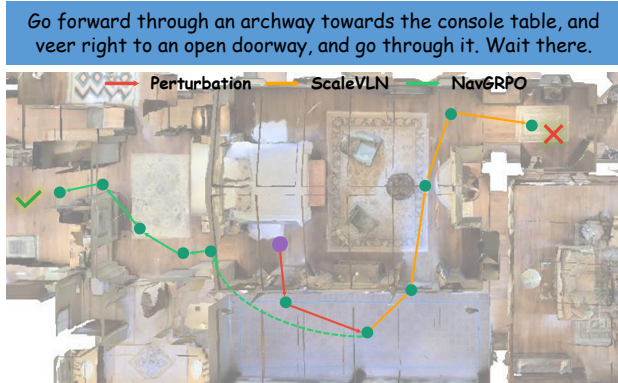


Figure 4. Qualitative comparison of navigation trajectories. Purple point indicates the starting location. NavGRPO’s trajectory (green) successfully completes the instruction by navigating through the archway and reaching the target doorway, while ScaleVLN’s trajectory (yellow) fails to execute the complete route, demonstrating NavGRPO’s superior robustness against environmental complexity.

memory burden of multi-trajectory optimization. The memory footprint scales linearly with rollout number K , doubling to 28.652 GB at $K=8$, representing a manageable and predictable scaling behavior. Training time per thousand steps increases moderately with K , yet our approach typically converges within 10k steps, maintaining reasonable total training cost while achieving improved performance. With $K=8$ achieving 72.65% SPL compared to ScaleVLN’s 69.97%, NavGRPO demonstrates a favorable performance-efficiency trade-off that justifies the moderate computational overhead.

10. Additional Visualizations

10.1. Qualitative Results

Figure 4 presents a representative navigation example that highlights the robustness differences between methods. Starting from the purple initial point, the agent must navigate through the archway toward the console table and then veer right to reach the open doorway. The red trajectory represents an initial perturbation that could mislead the agent. NavGRPO demonstrates stronger robustness by recovering from potential distractions and adhering to the instructional semantics, while ScaleVLN shows greater sensitivity to such perturbations. This qualitative observation aligns with our quantitative results, confirming that multi-trajectory optimization with balanced rewards enhances policy stability in complex navigation scenarios.

10.2. Failure Analysis

Figure 5 illustrates a challenging scenario where NavGRPO fails to reach the correct goal. The instruction requires the

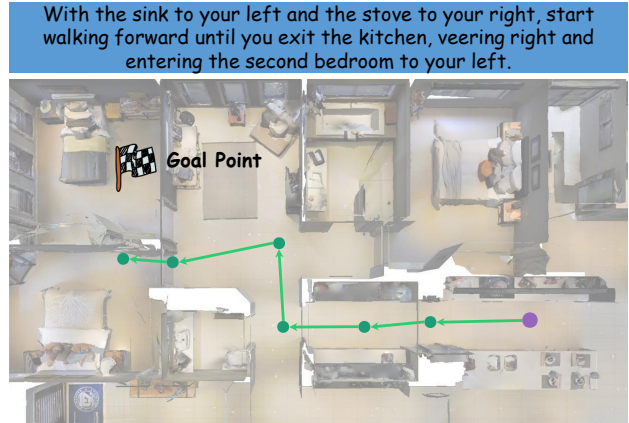


Figure 5. Failure case analysis. NavGRPO incorrectly interprets the spatial reference “second bedroom” in an instruction with multiple ambiguous directional cues, highlighting challenges in compositional spatial reasoning.

agent to navigate from the kitchen, veer right, and enter the second bedroom to the left. However, the spatial reference “second bedroom” is ambiguous given multiple visually similar bedroom entrances, and the conflicting directional cues “right” and “left” within the same instruction introduce additional complexity. The agent successfully exits the kitchen but misidentifies the target bedroom, revealing limitations in resolving compositional spatial relations across long-horizon instructions. This case underscores the challenge of grounding ambiguous linguistic spatial references in environments with repetitive structures, suggesting future directions in enhanced spatial reasoning and disambiguation mechanisms.

11. Limitations

Dependency on Base Model Quality. Our method fine-tunes pretrained vision-language models and inherits their limitations. When the base model exhibits systematic failures (e.g., misinterpreting certain spatial relations or object attributes), group-relative optimization may amplify rather than correct these biases, as all sampled trajectories suffer from the same foundational errors.